(SI)Structure and pair correlations of a simple Coarse Grained model for supercritical Carbon Dioxide

Bortolo Matteo Mognetti, Martin Oettel, Peter Virnau, Leonid Yelash, Kurt Binder

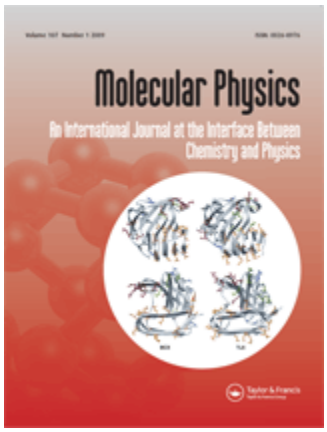

(SI)Structure and pair correlations of a simple Coarse Grained model for supercritical Carbon Dioxide

Journal:	*Molecular Physics*
Manuscript ID:	TMPH-2008-0443
Manuscript Type:	Special Issue Paper - Dr. Jean-Jacques Weis
Date Submitted by the Author:	30-Dec-2008
Complete List of Authors:	Mognetti, Bortolo; Mainz University, Institut für Physik Oettel, Martin; Mainz University, Institut für Physik Virnau, Peter; Mainz University, Institut für Physik Yelash, Leonid; Mainz University, Institut für Physik Binder, Kurt; Mainz University, Institut für Physik
Keywords:	Carbon Dioxide, Coarse Grained models, Supercritical Fluids
Note: The following files were submitted by the author for peer review, but cannot be converted to PDF. You must view these files (e.g. movies) online.	
manuscript.tar	

Structure and pair correlations of a simple Coarse Grained model for supercritical Carbon Dioxide

B. M. Mognetti[(a)], M. Oettel, P. Virnau, L. Yelash, K. Binder[(a)]

Institut für Physik, Johannes Gutenberg Universität Mainz,

Staudinger Weg 7, 55099 Mainz, Germany

A recently introduced coarse-grained pair potential for carbon dioxide molecules is used to compute structural properties in the supercritical region near the critical point, applying Monte Carlo simulations. In this model, molecules are described as point particles, interacting with Lennard-Jones (LJ) forces and an (isotropically averaged) quadrupole-quadrupole potential, the LJ parameters being chosen such that gratifying agreement with the experimental phase diagram near the critical point is obtained. It is shown that the model gives also a reasonable account of the pair correlation function, although in the nearest neighbor shell some systematic discrepancies between the model predictions and results from simulations of fully atomistic models and experiments are found. By comparison with results from an equivalent model but with the full angle-dependent quadrupolar interaction these discrepancies are traced back to the effect of orientational correlations and of the insufficient representation of molecular packing. Furthermore, the correlation length of density fluctuations is obtained from Ornstein-Zernike plots of the inverse structure factor, and shown to be in rough agreement with corresponding experimental results. Finally possible refinements of this coarse-grained model are briefly discussed.

(a) Electronic mail: mognetti@uni-mainz.de, kbinder@uni-mainz.de

I. INTRODUCTION

From the point of view of modern chemical engineering and processing supercritical fluids deserve a particular interest. Due to their peculiar properties [1] (e.g. strong density fluctuations) they are frequently used as plasticizer, solvent for polymers, blowing agents in foam forming etc. Among supercritical fluids, carbon dioxide (CO_2) is particularly in-

teresting because it is considered a green solvent [2] and its critical point ($T_c \approx 304$ K) is easily accessible. Its widespread use in the chemical industry is also a driving force for theoretical efforts aiming at the understanding of structural and bulk properties of pure CO_2 and mixtures containing it. Computer simulation techniques [3] such as the grand canonical Monte Carlo method [4, 5] naturally offer themselves as tools to obtain quantitative information in that direction. However, considering for instance the specific case of polymers dissolved in CO_2, severe practical difficulties appear related to the complicate topology of the phase diagrams [6, 7], the large number of degrees of freedom to sample (as, e.g., in an atomistic approach [8]), and the substantial number of control parameters (temperature, pressure, solvent concentration and chain length). These difficulties clearly set limitations in the practical determination of a precise mixture phase diagram which is required, e.g., in order to optimize the process of foam formation [9]. For this reason, the pursuit of a coarse grained description of the system in terms of only a few degrees of freedom appears to be an attractive way to proceed in the investigation of complex fluid mixtures [10, 11]. Coarse graining is well–established for polymers [11], naturally it should also be considered for solvent particles.

Recently [12, 13] we have proposed such a simple coarse–grained model for quadrupolar solvents (of which CO_2 is an example) which is able to reproduce nicely the corresponding experimental phase diagrams, as has been shown in particular for CO_2 and benzene (C_6H_6). Within this approach, the solvent molecules are modelled as Lennard–Jones (LJ) particles interacting with an additional electric quadrupole–quadrupole potential. The latter can either be considered in its full anisotropic form or in a spherically averaged form (thus adding a temperature–dependent, isotropic part to the LJ potential). The model possesses three parameters: the LJ particle radius, the LJ energy scale, and the quadrupole moment. The latter can be taken directly from experiment whereas the LJ radius and energy scale are determined by matching the critical point of the model to the experimental values of the solvent under consideration. (Note that this is different from previous attempts to fix the scale parameters in spherically averaged models [14].) Thus the model setup is suitably general and can be applied with modest effort to other quadrupolar solvents. The improvement with respect to previous attempts [15], which neglect explicit quadrupolar interactions, is significant not only in the quality of the phase diagram of the pure solvent but also in the calculation of the equation of state in mixtures with alkanes [16]. In the

latter case, no expensive experimental data for the mixture are necessary to fix the model since the polymer–solvent interaction parameters are determined by the Lorenz–Berthelot rule [3, 17].

The main investigation in [12, 13, 16, 18] was devoted to the equation of state of pure solvents and mixtures and shows that a good description of the phase diagram is achieved with a simple, single–bead representation of the solvent molecule. Considering the crude nature of this approximation (see Fig. 1), this is indeed surprising and may be viewed as the manifestation of a generalized "rule of corresponding states". However, away from coexistence, for high densities, deviations between the model and experimental equation of state for CO_2 could be observed [13] and can be related to an oversimplified treatment of the packing of the solvent molecules which is governed by the repulsive core of the intermolecular potential. In order to understand further the inevitable limitations of our modeling but also to obtain more insight as to the high quality of the equation of state near coexistence, we investigate in this work pair correlation functions and structure factors in the supercritical region. A second motivation is the already mentioned property of supercritical CO_2 as being a good solvent for other substances. This is related to strong density fluctuations, leading to cluster formation and encapsulation of solute molecules. Partly due to this engineering interest, there are a number of experimental and atomistic simulation studies available which offer rich possibilities for comparison.

We briefly outline the content of this work: In Sec. II we introduce the coarse–grained model and recall its equation of state. In Sec. III we present our main results for the structure in the supercritical region, using the spherically averaged model. This section is divided into two parts. In the first part the correlation length (governing the long-range behavior of the correlation functions) is discussed by comparing experimental data with a scaling analysis and simulations. In the second part, site–site and neutron–weighted correlation functions are compared to experiment and atomistic simulations. In Sec. IV we investigate the orientational correlations using the coarse–grained model with explicit quadrupolar interactions. Finally, in Sec. V we present our conclusions.

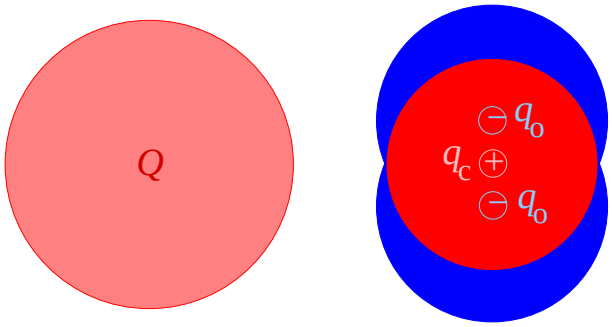

FIG. 1: (Color online) Schematic representation of the CO_2 molecule in the present coarse–grained model (left) and in a (still very simple) atomistic model (EPM (rescaled) [28], right). All spheres represent LJ beads, with diameter $\sigma = 3.784$ Å (left) vs. $\sigma_c = 2.757$ Å (carbon,right) and $\sigma_o = 3.033$ Å (oxygen, right). Our coarse–grained model assumes a pointlike quadrupole with moment $Q = 4.29$ DÅ at the center whereas the EPM (rescaled) model assigns partial charges $q_c = 0.651\,e$ to the carbon center and $q_o = -q_c/2$ to each of the oxygen centers.

II. THE COARSE–GRAINED MODEL

In Refs. [12, 13] we introduced the coarse–grained model with either explicit (point) quadrupolar interactions or spherically averaged quadrupolar interactions. With explicit quadrupolar interactions, the model pair potential between two CO_2 molecules is given by

$$V^F = 4\epsilon_F\left[\left(\frac{\sigma_F}{r}\right)^{12} - \left(\frac{\sigma_F}{r}\right)^{6} + S^0 - \frac{3}{16}q_F\sqrt{\left(\frac{\sigma_F}{r}\right)^{10} - \left(\frac{\sigma_F}{r_{\rm cut}}\right)^{10}}\,f^{QQ}\right] \quad , \tag{1}$$

$$q_F = \frac{Q^2}{\epsilon\sigma^5} \quad , \tag{2}$$

$$\begin{aligned} f^{QQ} &= 1 - 5\cos^2\Theta_i - 5\cos^2\Theta_j + 17\cos^2\Theta_i\cos^2\Theta_j + 2\sin^2\Theta_i\sin^2\Theta_j\cos^2(\Phi_i - \Phi_j) \\ &- 16\sin\Theta_i\cos\Theta_i\sin\Theta_j\cos\Theta_j\cos(\Phi_i - \Phi_j) \quad . \end{aligned} \tag{3}$$

In Eq. (1), the first contribution represents a cut–off and shifted LJ potential with $r_{\rm cut} = \sqrt[6]{2^7}\sigma_F \approx 2.24\sigma_F$ and $S^0 = 127/16384$ is chosen so that the LJ potential is zero at this distance. The second part characterizes the quadrupolar interaction, the angular dependence is given by f^{QQ} in Eq. (3) where (Θ_i, Φ_i) are the polar angles characterizing the orientation of the uniaxial molecule relative to the axis connecting the sites $\vec{r}_i, \vec{r}_j$ of the two particles. The (physical) quadrupole moment Q (in CGS units) is connected to a dimensionless quadrupole moment q_F via Eq. (2). The peculiar form of the cut–off dependence of the quadrupolar part facilitates the spherical average $\beta V = -\ln\langle\exp(-\beta V^F)\rangle_{\Theta_i,\Phi_i}$. The leading term in its

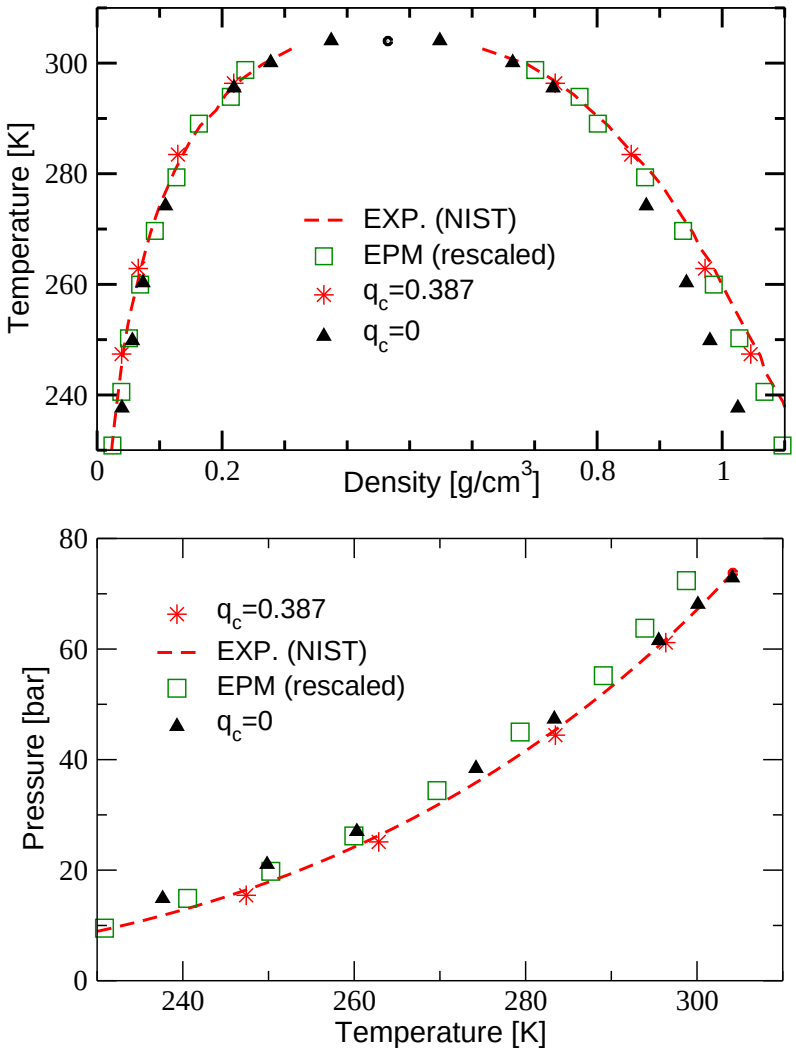

FIG. 2: (Color online) Phase diagram of CO_2 [coexistence densities (a) and pressure (b)] as obtained in Ref. [13]. The dashed line corresponds to experimental results according to the NIST parametrization [20]. Stars give the results for the spherically averaged model (Eq. (4)), squares correspond to the EPM (rescaled) model as introduced in Ref. [28], and triangles correspond to a pure LJ fluid [15].

high temperature expansion results in an attractive contribution $\propto r^{-10}$ (see also [14, 19]). Using this result, the pair potential of the spherically averaged model is given by:

$$V^A = 4\epsilon\left[\left(\frac{\sigma}{r}\right)^{12} - \left(\frac{\sigma}{r}\right)^{6} - \frac{7}{20}q_c\frac{T_c}{T}\left[\left(\frac{\sigma}{r}\right)^{10} - \left(\frac{\sigma}{r_{\rm cut}}\right)^{10}\right] + S^0\right] \quad , \tag{4}$$

$$q_c = \frac{Q^4}{\epsilon k_B T_c \sigma^{10}} \quad , \tag{5}$$

The central idea in our approach is to fix the free parameters of the two models defined above by the experimental values of the critical point of CO_2 ($T_c = 304.13$ K, $\rho_c = 10.62$ mol/ℓ) [12, 13]. For a given value of the quadrupole moment Q (fixed by experiment), this results in different values for the energy and length scales ϵ_F, σ_F (model with explicit quadrupolar interactions) and ϵ_A, σ_A (spherically averaged model). Explictly, we obtain for $Q = 4.292$ DÅ (experimental value $Q = 4.3 \pm 0.4$ DÅ [20]) the following set of parameters for the explicit quadrupolar model defined by Eq. (3)

$$\epsilon_F = 3.598 \times 10^{-21}\,\text{J} \qquad \sigma_F = 3.760\,\text{Å} \qquad q_F = 0.689 \quad . \tag{6}$$

Using the same value for Q, we obtain for the spherically averaged model defined by Eq. (4)

$$\epsilon_A = 3.494 \times 10^{-21}\,\text{J} \qquad \sigma_A = 3.784\,\text{Å} \qquad q_c = 0.385 \quad . \tag{7}$$

(For the non–trivial numerical procedure to fix these parameters, see Refs. [12, 13].)

In Fig. 2 we recall results for the phase diagram of CO_2 [13]. The binodal of the spherically averaged model is almost indistinguishable from the experimental one. The binodal of a particular example of an atomistic model (EPM rescaled, see Ref. [28] and Fig. 1) is of similar quality, however, the coexistence pressure is slightly less well described by the latter. For comparison, we also show the binodal of a pure LJ model with energy and length scale again adjusted to the critical point of CO_2 ($\epsilon_{\rm LJ} = 4.206 \times 10^{-21}$ J, $\sigma_{\rm LJ} = 3.695$ Å [15]) which clearly deviates from the experimental curve. Since all models whose binodals are shown here have been adjusted to the experimental critical point, one can draw the conclusion that for a correct description of phase coexistence the use of a spherically averaged model with a *temperature dependent part* (corresponding to the physical quadrupole) in the effective two–particle potential is sufficient. It does not seem to be necessary to insist on atomistic details, note furthermore that such a temperature dependent interaction would also be obtained if one averages over the pair potential of the atomistic model. Note that due to the presence of

explicit (partial) charges in the atomistic model, the use of the latter would be inconvenient for a study of the critical behavior (see Sec. III) or when one considers the phase behavior of mixture of CO_2 with alkanes (see Ref. [16]).

III. CO_2 IN THE SUPERCRITICAL REGION

In this section we investigate the correlation length and site–site pair correlation functions of carbon dioxide in the supercritical region. We will compare to experimental data for the correlation length [21, 22] obtained for supercritical temperatures in the range $T/T_c - 1 = 2.3 \cdot 10^{-3} \ldots 3.7 \cdot 10^{-2}$ (Subsec. III A). Experimental and atomistic simulation data for the site–site correlation functions have been obtained in Refs. [23, 24] for two temperatures $T = 307$ K ($T/T_c = 1.01$) and $T = 310$ K ($T/T_c = 1.02$) and several densities. The corresponding comparison with our model will be discussed in Subsec. III B.

A. Correlation length

The correlation length ξ reflects the range of the asymptotic decay of the pair correlation function $g(r)$. For a fluid with short–ranged interactions, its practical determination is almost exclusively facilitated through the analysis of the small–q behaviour of the structure factor (Ornstein–Zernike plots):

$$S(q) \stackrel{q\to 0}{=} \frac{S(0)}{1+\xi^2 q^2} \qquad S(q) = 1 + \rho \int \mathrm{d}\mathbf{r} \exp(i\mathbf{rq}) \Big[g(r) - 1 \Big] \quad . \tag{8}$$

This assumed form of $S(q)$ corresponds to a long–ranged decay of the pair correlation function $g(r) \to 1 + \exp(-r/\xi)/r$ [25]. Although the critical behaviour of the Ising model (defining the universality class under which also fluids with short–ranged interactions are assumed to fall) is slightly different ($g(r) \to 1 + \exp(-r/\xi)/r^{1+\eta}$ with $\eta \approx 0.036$), the deviations of the corresponding $S(q)$ from the form in Eq. (8) are small for practical purposes.

First we consider the results presented in Ref. [21], where experimental results for the structure factor, obtained using small-angle neutron scattering (SANS), have been given for five supercritical states very near the critical point ($T/T_c - 1 = 0.0023 \ldots 0.0033$). In Ref. [21] a reverse Monte Carlo method was used to fit SANS intensities, from which the correlation length ξ was obtained using Eq. (8).

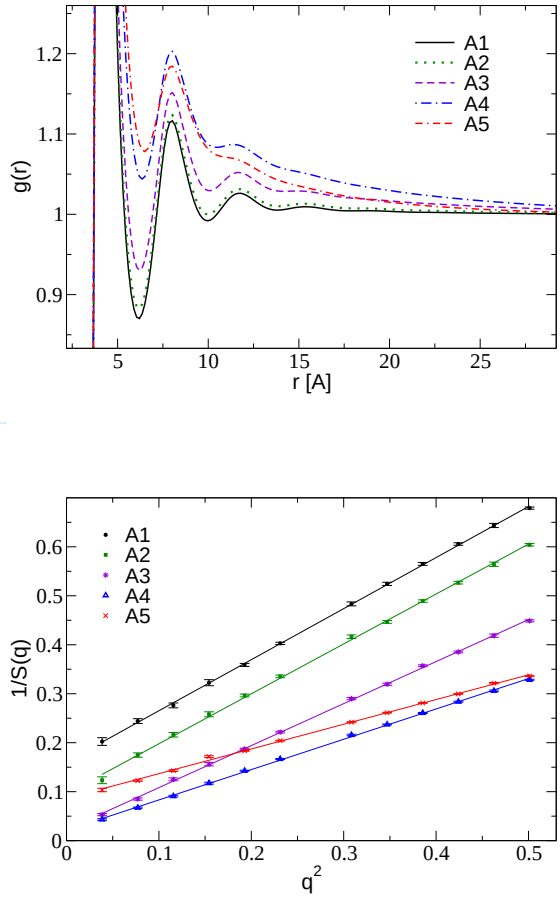

FIG. 3: (Color online) Pair correlation functions $g(r)$ and inverse structure factors $S(q^2)^{-1}$ at low q^2 (in σ_A^{-2} unit) for the five state points A1...A5 investigated in Ref. [21], see also Table I.

At the five thermodynamic points reported in Ref. [21], we have performed massive NVT Monte Carlo Simulations [4] of the spherically averaged model (Eq. (4)). We use cubic boxes of size $(121\cdot\text{Å})^3$ with the number of particles being between 6,780 and 15,673. Monte Carlo moves consist in simple local rearrangement of particle positions, and near criticality "critical slowing down" limits the accuracy that can be reached. In a run equivalent of 4,800 h per AMD Opteron DualCore 2.6 GHz processor, and estimating the autocorrelation length using the binning methods, we are confident, however, that a reasonable number of uncorrelated configurations have been generated. Results for the pair correlation functions $g(r)$ and inverse structure factors $S(q^2)^{-1}$ at low q^2 for the five points investigated in Ref. [21] are shown in Fig. 3. As can be seen, our data for $S(q^2)^{-1}$ can be fit very well with a straight line, permitting the extraction of the correlation length ξ. The results for ξ in comparison

State	T [K]	p [bar]	ρ [g/cm^3]	ξ [Å]
critical point	304.25 [304.128]	73.8	0.468	-
A1	305.25	79.7	0.645	12.9 [9.5(1)]
A2	305.05	77.6	0.620	16.2 [13.4(4)]
A3	305.15	75.7	0.538	42.1 [25(2)]
A4	304.95	74.6	0.362	20.5 [22.9(5)]
A5	305.05	72.4	0.279	11.1 [9.6(3)]

TABLE I: Equation of state and correlation length for the equilibrium states reported in [21]. In square brackets we report results of the present work obtained fitting results of Fig. 4 for $(q \cdot \sigma_A)^2 < 0.25$. In bracket we report statistical error which amounts to almost 6%. On the other hand repeating the fits for $q^2 < 0.5$ we observe systematic discrepancies up to 12%. For this reason we estimate that our results should be trusted within 15% errorbars. We note that the critical point which we use is 0.04% below the measured one in [21].

to the experimental data is given in Table I. Simulations and experimental results are in qualitative agreement, however, some quantitative disagreements for densities $\rho > \rho_c$ are present. There the correlation length from simulations appears to be systematically lower. In order to gain a better understanding of the global behavior of $\xi(T, \rho)$ and of possible sources of error we have performed a phenomenological scaling analysis, using non–universal critical amplitudes for CO_2 [26] coupled with universal ratios [27] (see App. A). The data of Ref. [21], our simulation results and the results of the scaling analysis are compared in Fig. 4(a). Our simulation results appear to be consistent with the scaling analysis, except for the point with reduced density 0.15. For this point, systematic errors in the Monte–Carlo results, related to finite size effects, become more and more important while error-bars take into account only statistical fluctuations (see the discussion in Table I). For $\rho > \rho_c$, the finding of an experimental ξ which is higher than that of the scaling analysis seems to be persistent also for a different set of experimental data [22], see Fig. 4(b). It is difficult to give a final conclusion in view of the unknown experimental uncertainties in determining densities and temperatures, but it appears possible that for $\rho > \rho_c$ sizeable non-universal corrections are present. Note that there are no predictions of ξ near criticality from simulations of the atomistic EPM model to compare with, since such simulations would require quite large

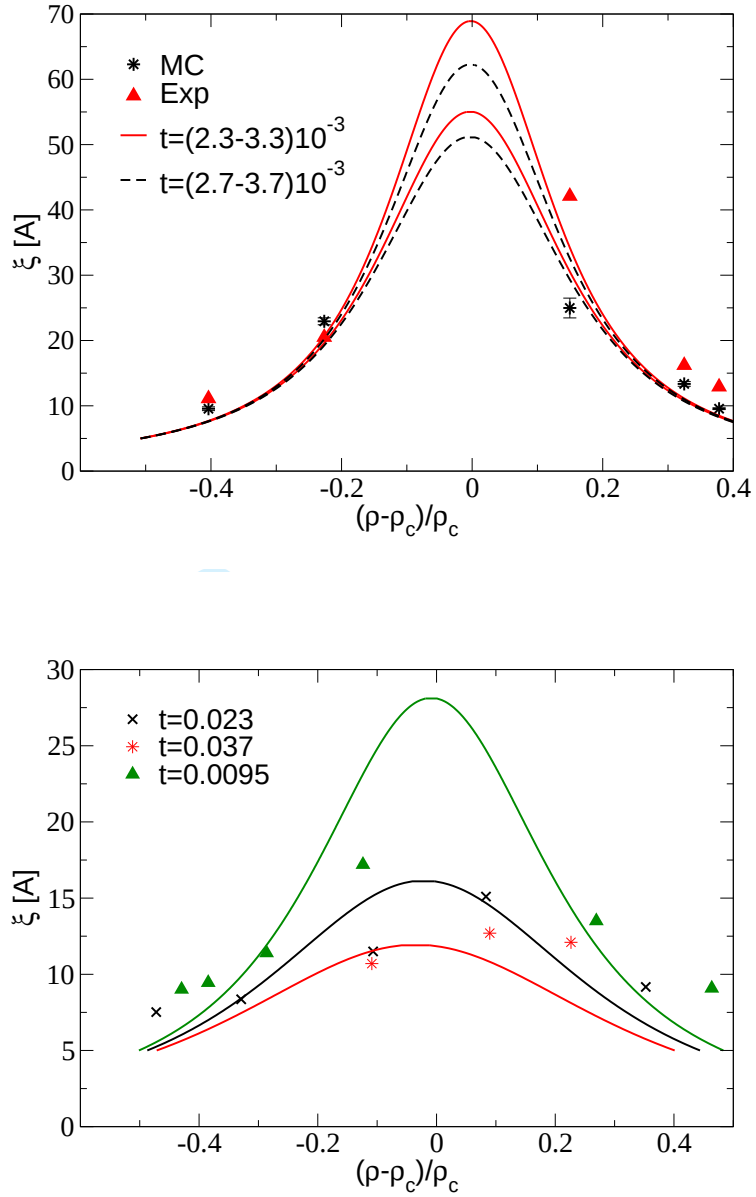

FIG. 4: (Color online) (a) Experimental results for ξ [21] compared with our simulations and the scaling analysis of App. A Simulations and experiments have been done at the same physical temperature T. However, Ref. [21] uses a critical temperature which is slightly different from the value which we use. Therefore, broken ($T_c = 304.128$ from our simulation) and full lines ($T_c = 304.25$ K from experiment) [21]) give results according to the scaling analysis with $t = (T - T_c)/T_c$ calculated accordingly. The MC errorbars reported are statistical ones, while we expect (as discussed in Table I) systematic error which validate our results within a 15% level of confidence. (b) Experimental results for ξ according to Ref. [22] compared with the scaling analysis.

	B1	B2	B3	C1	C2	C3	C4	D1	D2	D3
T [K]	307	307	307	310	310	310	310	313	373	373
ρ [g/cm^3]	0.2	0.468	0.6	0.15912	0.36036	0.5616	0.702	1.023	0.943	0.833

TABLE II: State points investigated in Ref. [24] (for T=307 K, named B1-B3), in Ref. [23] (for T=310 K, named C1-C4) and in Ref. [30] (D1-D3).

computational efforts.

B. Site–site correlation functions

In a second comparison, we will focus on the short–ranged correlations as seen in the peak structure of site–site correlation functions [where the sites can be either carbon (C) or oxygen (O)]. We consider the results reported in [23, 24] for two isotherms (see Table II). In [24] neutron weighted radial distribution functions and corresponding molecular dynamic simulations (using the EPM (rescaled) model [28]) of three state points (B1...B3 in Table II) have been reported. In ref. [23] neutron weight radial distribution functions are also given (for the four states C1...C4 in Table II) along with simulations results obtained using the model of Murthy et al. [29]. In both cases, the atomistic models gave a good account of the experimentally determined neutron weighted $g(r)$.

For the states investigated in [23, 24], we have done NVT simulations using the averaged model (4). In Fig. 5 (full lines) we report pair correlation function $g(r)$ of the spherically averaged model (4) compared with (dot lines) C–C pair correlation functions numerically obtained in [24] (state points B1...B3 , T=307 K) and [23] (state points C1...C4 , T=310 K). Compared to the atomistic models, we find that the position of the first and the (weak) second peak are reproduced whereas the first peak is too narrow and high in our averaged model. Here, the assumption of a single LJ bead of the averaged model is too rigid and does not account properly for the side–to–side configuration of two CO_2 molecules. The inadequacy of the repulsive part of the single–bead LJ potential can also be seen if one does a spherical average of the atomistic potential of the EPM (rescaled) model (for its definition, see Fig. 1). Whereas the potential minimum coincides with the one in our model, the repulsive part of the EPM (rescaled) averaged potential is much softer.

In [23], atomistic simulation results for the carbon-oxygen [$g_{CO}(r)$] and oxygen-oxygen

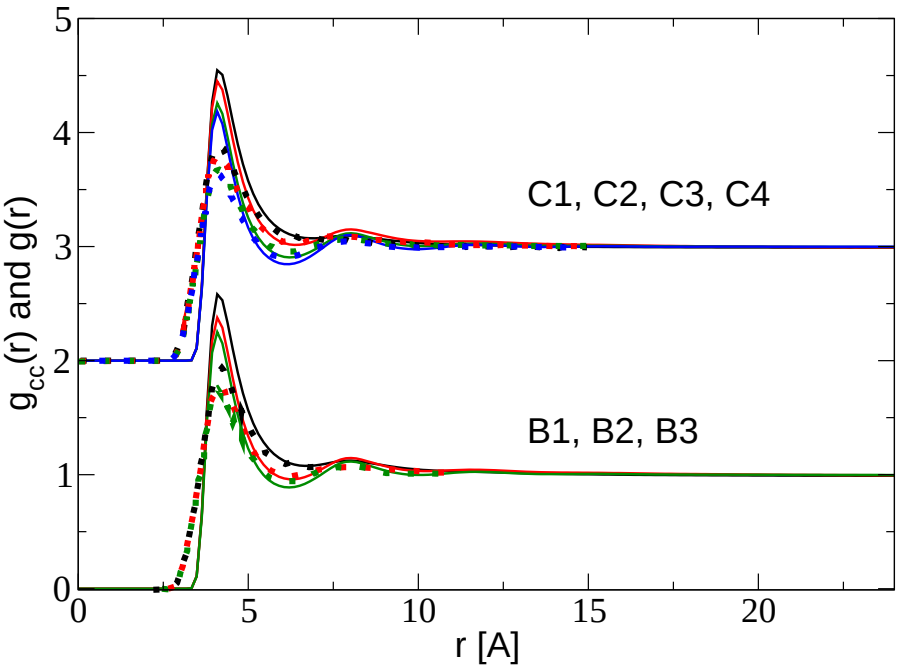

FIG. 5: (Color online) Full lines: pair correlation functions of the model investigated in this paper, for the two isotherm of Table II. Dotted lines: results for the carbon-carbon correlation functions for the two isotherms of the Table II obtained in [23, 24] (see the text for more detail). Curves with higher first peak correspond to states with lower density.

$[g_{OO}(r)]$ correlation functions have also been reported (dotted lines in Fig. 6). Of course the latter cannot be measured in our simple model which neglects all atomistic details. However, a simple reconstruction procedure for these correlation functions is suggested as follows. Compared to g_{CC} (Fig. 5), we can observe that $g_{CO}(r)$ and $g_{OO}(r)$ exhibit the same position for the peaks which are however less prominent and more dispersed. This spatial dispersion is due to the spatial fluctuations of the oxygen atoms near the carbon center of mass. We assume a rigid, linear model for the CO_2 molecule, with the distance between carbon and oxygen atoms given by the experimental value $d_{CO} = 1.19$Å. Correspondingly, the distance between the two oxygen atoms is given by $d_{OO} = 2d_{CO}$. Furthermore, we identify $g_{CC}(r)$ with our $g(r)$ and obtain $g_{CO}(r)$ and $g_{OO}(r)$ by averaging over the orientations of the molecules,

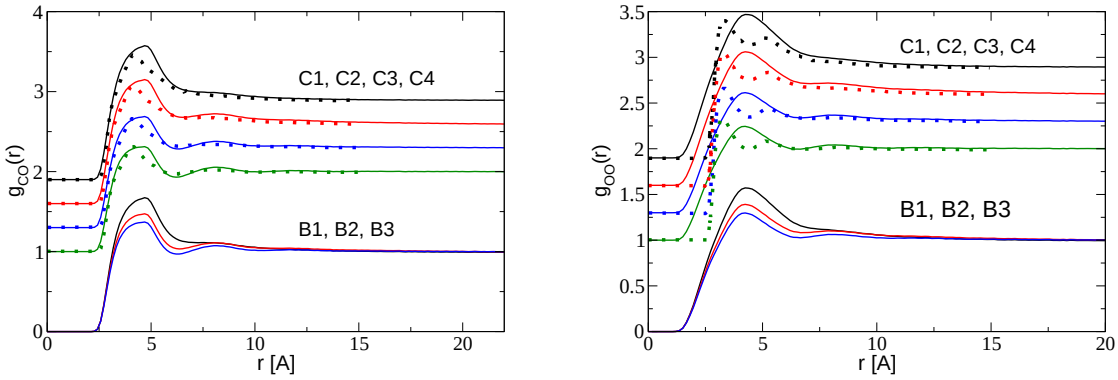

FIG. 6: (Color online) a) Full lines: carbon-oxygen pair correlation functions of the model investigated in this paper, for the two isotherms of Table II. Dotted lines: results for the carbon-oxygen correlation functions for the $T = 310$ K isotherm obtained in [23]. Curves with higher first peak correspond to states with lower density. b) The same as in Fig. 6b) for the oxygen-oxygen correlation functions.

weighted properly by $g(r)$:

$$g_{CO}(r) = \int \frac{\mathrm{d}\mathbf{w}_1 \mathrm{d}\mathbf{w}_2 \mathrm{d}\mathbf{r}'}{4\pi r^2} g(r')\delta(d_{C_1O_2} - r) \qquad g_{OO}(r) = \int \frac{\mathrm{d}\mathbf{w}_1 \mathrm{d}\mathbf{w}_2 \mathrm{d}\mathbf{r}'}{4\pi r^2} g(r')\delta(d_{O_1O_2} - r)\,. \tag{9}$$

In Eq. (9), $\mathbf{w}_1$ and $\mathbf{w}_2$ are the unit vectors pointing from C to O on each molecule, $d_{C_1O_2}$ is the distance between the carbon atom of the first molecule and one oxygen atom of the second molecule which can be obtained as a function of $\mathbf{w}_i$, r' (the distance between the carbon atoms) and d_{CO} using simple trigonometric relations. $d_{O_1O_2}$ is the distance between two oxygen atoms on different molecules and is computed similar to $d_{C_1O_2}$. $\mathbf{w}_1$ and $\mathbf{w}_2$ are sampled uniformly (and independently) on the unit spheres.

In Fig. 6 we report our approximation for g_{CO} and g_{CC} (full lines), compared with the results of ref. [23] (dotted lines). The qualitative shape of the results of the atomistic simulations [23] is reproduced (such as the height of the peaks), but rather big discrepancies in g_{OO} remain. At short distances, in the case of $g_{OO}(r)$, the results from the atomistic simulations go to zero faster than our predictions, oppositely to what happens in g_{CC} (5). For this reason we argue that the rather good agreement in $g_{CO}(r)$ is merely a fortunate cancellation of errors. For $g_{OO}(r)$ (Fig. 6b), the atomistic models predict a double peak structure that our approach ignores. This effect is due to orientational correlations which

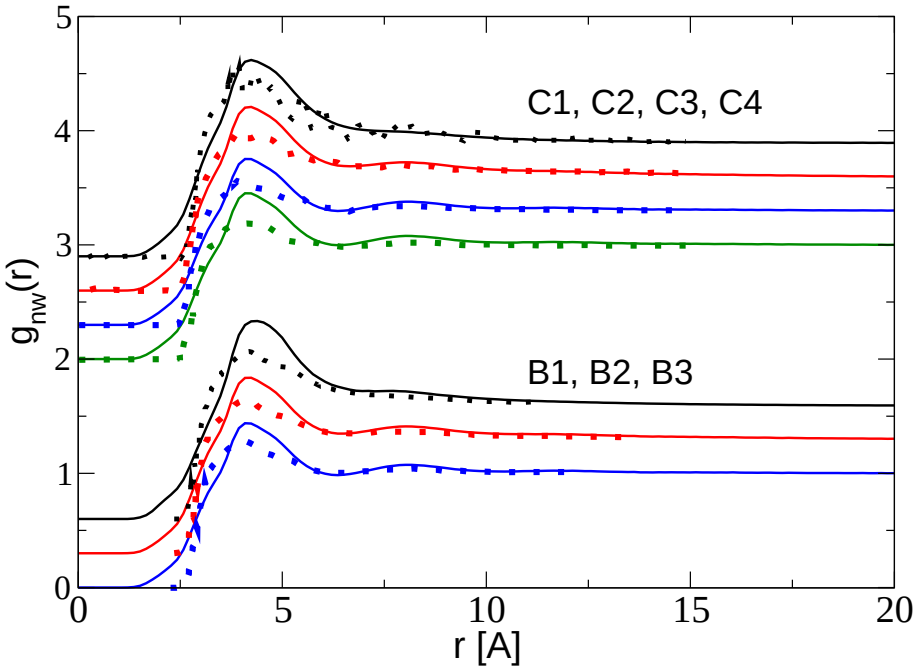

FIG. 7: (Color online) Dotted line: experimental neutron weighted pair correlation functions of refs. [23, 24], for the seven thermodynamic states reported in Table II. Full lines: simulation estimate of the neutron weighted pair correlation function using formula (10) (see ref. [30]). Curves with higher first peak (i.e. from the top to bottom) correspond to states with lower density.

are neglected in our approach. The orientational correlations imply that CO_2 molecules at small distances (in the first solvation shell) prefer to stay in a T-shape configuration (i.e. with the two molecules axes orthogonal $\mathbf{w}_1 \cdot \mathbf{w}_2 = 0$), which minimizes the quadrupolar quadrupolar interaction (1). If we put two molecules in a T-shape configuration with the distance between carbon atoms equal to 5Å (as suggested by the position of the first peak in Fig. 5) and we measure the two intermolecular distances between oxygen atoms we obtain 3Å, and 6Å corresponding approximately to the position of the two peaks in Fig. 6.

Finally we can compare our results with correlation functions obtained using neutron weighted experiments. For such a comparison, the neutron weighted pair correlation function must be compared with the following combination of atomistic pair correlation function [30]

$$g_{nw} = 0.133 g_{CC} + 0.464 g_{CO} + 0.403 g_{OO} \quad . \tag{10}$$

Using our results (Figs. 5, 6) (keeping in mind the limitation of our approach that we have just pointed out), the results for g_{nw} together with the experimental results reported in Refs. [23, 24] is shown in Fig. 10. We observe that the simulation results (full lines) systematically overestimate the experimental peak, due to the overestimated peak in $g_{CC}(r) \equiv g(r)$. We observe also that the core region is reached more steeply in the experimental results than in our simulation data. This is related to the deficiencies of our $g_{OO}(r)$ for 1.5Å$\leq r \leq$4Å, which has been discussed before. Our results imply that an excellent fit of the equation of state, as achieved by our model potential [12, 13], does not guarantee a similarly accurate prediction of the local structure of the fluid.

IV. ORIENTATIONAL STRUCTURE

In the previous section we have pointed out the importance of considering orientational correlations in describing the structure of carbon dioxide at small distances ($r \leq 7$Å). These were for instance responsible for the double peak structure in the oxygen-oxygen pair correlation function (Fig. 6) which was not properly reproduced by the averaged model V^A (Eq. (4)). In this section we present results for the model with explicit quadrupolar interactions [Eq. (1)] with parameters given in Eq. (6). This model with explicit angular dependency was already considered in Ref. [13] where, among other things, we compared the phase diagram of CO_2 as obtained using V^F or V^A. Both phase diagrams turned out to be very similar, with the spherically averaged model showing even better agreement with experiment than the explicit model.

Lennard-Jones potentials plus point-like quadrupolar interactions have been a long-time subject of investigation (see eg. [31]), both by simulation and using equation of states. In such investigations the full (angular-dependent) pair correlation function $g(\mathbf{r}, \mathbf{w}_1, \mathbf{w}_2)$ (where $\mathbf{r}$ is the intermolecular vector, $\mathbf{w}_1$ and $\mathbf{w}_2$ are the orientations of the linear molecules) is projected onto spherical harmonics in a proper reference systems (usually the laboratory frame or the molecular frame in which the orientation of a molecule is fixed). Following Ref. [31], in the laboratory reference frame (i.e. with the orientations of the two molecules

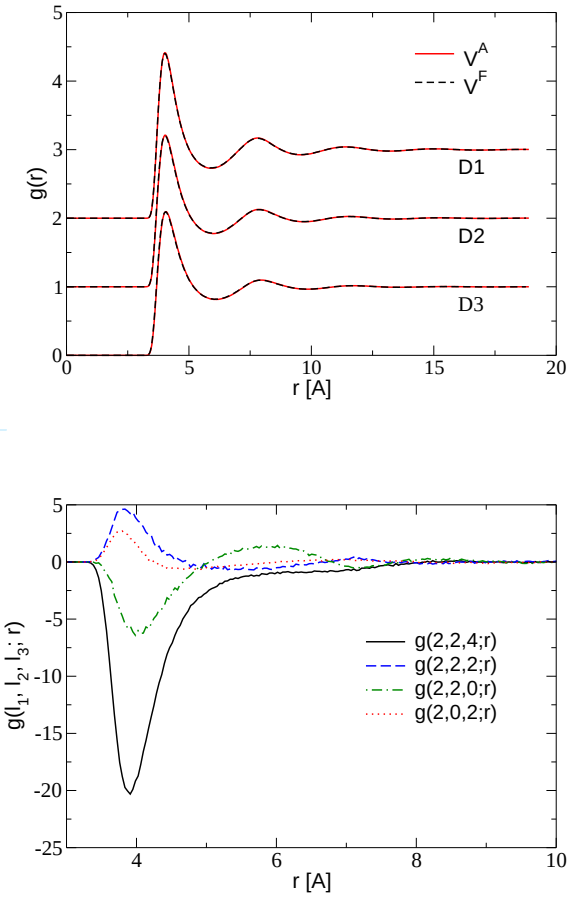

FIG. 8: (Color online) (a) Pair correlation functions using the averaged V^A (full lines) and the full V^F (broken lines) model for the state points D1, D2 and D3 (see Table II). In the statistical errors the two models predict the same results. (b) Harmonic decomposition of the pair correlation function for the full model V^F in the laboratory reference frame [see Eq. (11)]. Angular correlations are well visible in the first and second solvation shell [see Fig. 8(a)], while for $r > 8$Å $g(l_1, l_2, l; r)$ is almost zero.

free) $g(l_1, l_2, l; r)$ are defined in the following manner

$$g(\mathbf{r}, \mathbf{w}_1, \mathbf{w}_2) = \sum_{l_1 l_2 l} g(l_1, l_2, l; r) \sum_{m_1 m_2 m} C(l_1, l_2, l; m_1, m_2, m) \tag{11}$$

$$Y_{l_1,m_1}(\mathbf{w}_1) Y_{l_2,m_2}(\mathbf{w}_2) Y^*_{l,m}(\mathbf{w}) \quad , \tag{12}$$

where $C(l_1, l_2, l; m_1, m_2, m)$ are Clebsch–Gordan coefficients, $\mathbf{r} = r\mathbf{w}$, and $Y_{l,m}(\mathbf{w})$ spherical harmonics. For isotropic potentials (like V^A), $g(l_1, l_2, l; r)$ are strictly zero apart from $g(0, 0, 0; r)$ which corresponds to the standard pair correlation function (up to a normaliza-

tion factor related to the chosen reference frame).

Monte Carlo results for the model with explicit quadrupolar interactions have been obtained for the three state points D1...D3 (see Table II) which have been investigated in Ref. [30] experimentally and by atomistic simulations using an EPM–like model. In Fig. 8(b) we report several $g(l_1, l_2, l; r)$ for the state point D1 for which $T \approx T_c$ and $\rho \approx 2.2\rho_c$. We can see that orientational correlations are well visible at this rather high density, especially in the first solvation shell (while they are much weaker in the second shell). On the other hand it is interesting to observe how concerning the pair correlation function [Fig. 8(a)] the full model (1) and the averaged model (4) predict almost the same results for all the three state points D1...D3. Incidentally, the same result holds for state points at coexistence. Indeed we have verified that the pair correlation functions in the coexistence liquid branch are almost equal for the explicit (V^F) and averaged (V^A) model (in this case minimal differences are visible only in the height of the first peak).

Angular anisotropies in the pair correlation function can be conveniently monitored using the partially averaged pair correlation function

$$g(r, \theta) = \int d\mathbf{w}_2 g(\mathbf{r}, \mathbf{w}_1, \mathbf{w}_2)$$

where $\cos\theta = \mathbf{w} \cdot \mathbf{w_1}$. It describes the probability to find a second molecule at distance r and angle θ with the z–axis provided the first molecule is fixed at the origin with orientation along the z–axis. For the state point D_1 our result for $g(r, \theta)$ is shown in Fig. 9 and clearly shows the presence of angular anisotropies (preferential arrangement of the second molecule near the "poles" and the "equator" of the sphere defined by $\mathbf{w_1}$). Thus we reproduce qualitatively the same phenomena observed in atomistic models (see also Refs. [32, 33]). Quantitative differences remain however: the atomistic simulation in Ref. [30] (see Fig. 6(a) in the third work) predict a more pronounced peak around the equator ($\cos\theta = 0$), similar to other investigations [32, 33]. At this point we should also mention that at high pressure and high density (as considered in states D in Table II), the deficiency of our coarse–grained models related to the inadequate repulsive part of the potential reaches up to 5% in the equation of state. Further systematic improvements of our coarse–grained model aiming at quantitative reproduction of anisotropic structure data should therefore include a more systematic partial angular averaging of more realistic, atomistic potentials.

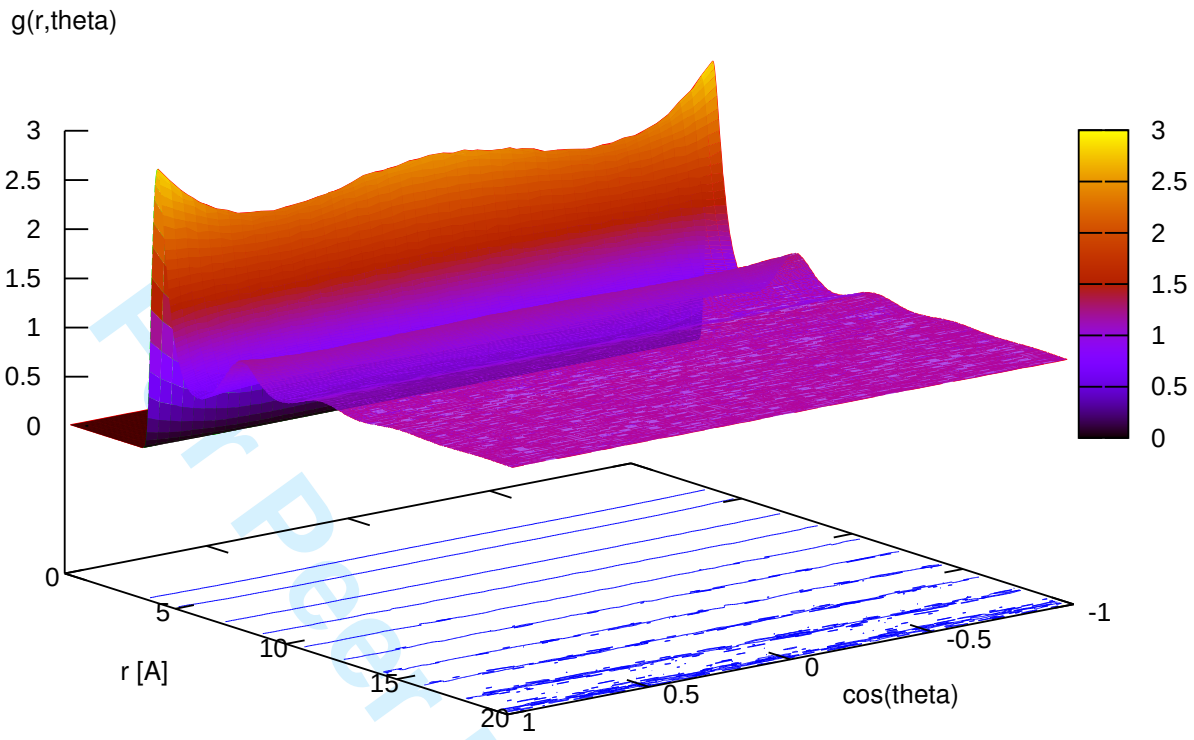

FIG. 9: (Color online) Pair correlation function $g(r, \theta)$ as a function of the intermolecular distance r and the angle θ between the molecular axis and the intermolecular direction ($\cos\theta = \mathbf{w} \cdot \mathbf{w_1}$). The plot refers to state D1 of Table II.

V. CONCLUSION

In this paper we have investigated the correlation length and correlation functions (site–site and angular–resolved) of carbon dioxide (CO_2) in the supercritical region for an efficient coarse–grained model defined by single Lennard–Jones beads with additional point quadrupolar interactions (taken into account explicit or spherically averaged). This model gives good results for pure component phase diagrams (e.g. CO_2 and C_6H_6) [12] and in the phase diagrams of mixture with alkanes [16]. Its performance for structural properties gives a more differentiated picture. At small distances ($r < 8$Å) the pair correlations of CO_2 are mainly given by packing effects. These are not correctly taken

into account by our coarse–grained model which neglects atomistic details and maps the CO_2 molecule insufficiently onto a spherically symmetric, single bead. Indeed looking at the first solvation shell of the center of mass pair correlation function (see Fig. 5), our model predicts a too narrow and too high peak in comparison with the predictions of atomistic models [23, 24], while the position of the peak is properly reproduced. On the other hand in the long distances regime (and near the critical point) physics is driven by long range fluctuations which happen at the scale of the correlation length ξ. Using an Ornstein-Zernike fit, we have computed the correlation length for several states near the critical point. Results are in qualitative agreement with experiment and scaling predictions (see App. A). Possible explanations of quantitative discrepancies have been discussed. Note that correlation lengths near criticality are notoriously difficult to estimate by simulations, and no such simulation estimates from more realistic atomistic models of CO_2 are available. We have also investigated explicit angular correlations in the coarse-grained model. For the phase diagram, there is substantial agreement between the spherically symmetric model and the model with explicit quadrupolar interactions [13]. This agreement is also reflected in the pair correlation functions: $g(r)$ from the spherically averaged model and the isotropic component of $g(\mathbf{r}, \mathbf{w}_1, \mathbf{w}_2)$ from the model with explicit quadrupolar interactions are the same within statistical errors for the state points investigated here.. We have found that the explicit model is able to qualitatively reproduce anisotropies in the first solvation shell which are usually discussed in the literature employing atomistic models.

ACKNOWLEDGEMENTS

B.M.M. thanks the BASF AG (Ludwigshafen) for financial support, while M.O. was supported by the Deutsche Forschungsgemeinschaft via the Collaborative Research Centre (Sonderforschungsbereich) SFB-TR6 "Colloids in External Fields" (project section N01). CPU times was provided by the NIC Jülich and the ZDV Mainz. Useful and stimulating discussion with F.Heilmann, L.G.MacDowell, M.Müller, W.Paul, H.Weiss and J.Zausch are gratefully acknowledged.

APPENDIX A: SCALING PREDICTION FOR THE CORRELATION LENGTH IN THE SUPERCRITICAL REGION

In this appendix we report the procedure that has been used to obtain the scaling predictions for the correlation length ξ near the critical point. Renormalization group theories [34] predict that the scaling laws of thermodynamic quantities (specific heats, correlation length, etc.) do not depend on atomistic details of the system but are the same within certain universality classes (the Ising one for the gas-liquid transition) [35]. We define the reduced density $\widehat{\rho}$ and temperature t [35]

$$\widehat{\rho} = \frac{\rho - \rho_d(t)}{\rho_c} \qquad t = \frac{T - T_c}{T_c} \quad , \tag{A1}$$

where ρ_d is the coexistence diameter $\rho_d(t) = (\rho_l^c + \rho_g^c)/2$ (ρ_l^c and ρ_g^c liquid and gas coexistence densities) extrapolated also into the supercritical region. Standard scaling relations are written as (for $\widehat{\rho} = 0$)

$$\xi = f_+ t^{-\nu} \quad (t \to 0^+) \tag{A2}$$

$$\xi = f_- (-t)^{-\nu} \quad (t \to 0^-) \tag{A3}$$

$$\widehat{\rho}_{l/g} = \pm B(-t)^{\beta} \tag{A4}$$

and (for $t = 0$)

$$\xi = \xi_c |\widehat{\mu}|^{-\nu_c} \tag{A5}$$

$$|\widehat{\mu}| = D_c |\widehat{\rho}|^{\delta} \tag{A6}$$

$$\xi = \xi_c D_c^{-\frac{\nu}{\beta\delta}} |\widehat{\rho}|^{-\frac{\nu}{\beta}} \quad , \tag{A7}$$

where (A7) has been obtained using Eqs. (A5) and (A6) and known relations on critical exponents [27], while $\widehat{\mu}$ is the reduced chemical potential. In Eqs. (A2)-(A7) the exponents are universal quantities, proper of the Ising universality class, while the amplitudes are system dependent. On the other hand renormalization group also predicts that certain adimensional ratios of amplitudes are also universal. This is a big simplification because it reduces the set of experimental input required for the scaling analysis. Ref. [27] reports the following best estimates for critical exponents

$$\delta = 4.789(2) \qquad \eta = 0.0364(5) \qquad \beta = 0.3265(3) \qquad \nu = 0.6301(4) \quad , \tag{A8}$$

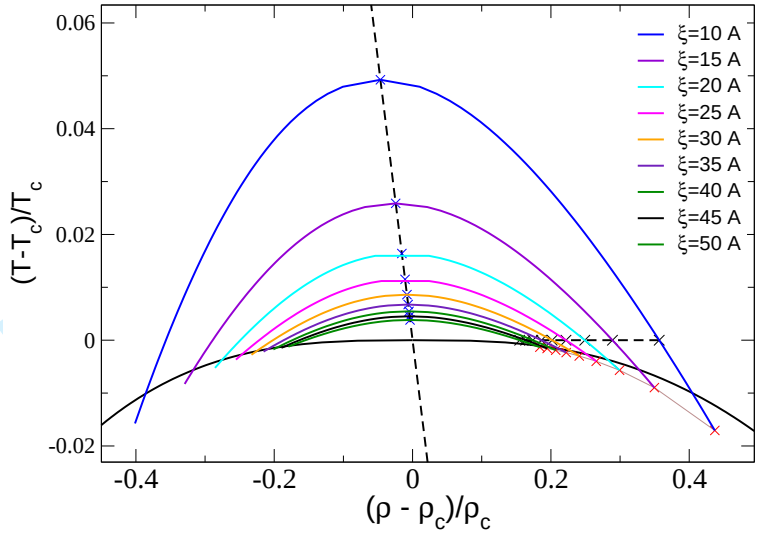

FIG. 10: (Color online) Lines at constant correlation length (from 10Å to 50Å) in the reduced density-temperature planes. The broken line is the coexistence diameter (extrapolated into the supercritical region)

while for the universal amplitudes in the present investigation we use [27]

$$\mathbf{U}_\xi = \frac{f_+}{f_-} = 1.95(2) \qquad [36] \tag{A9}$$

$$\mathbf{Q}_2 = \left(\frac{\xi_c}{f_+}\right)^{2-\eta} \frac{\Gamma}{\Gamma_c} = 1.17(2) \qquad [37] \tag{A10}$$

$$\mathbf{R}_\chi = D_c \Gamma B^{\delta-1} = 1.7(3) \qquad [38] \tag{A11}$$

$$\mathbf{1} = \Gamma_c \delta D_c^{\frac{1}{\delta}} \tag{A12}$$

where "capital gammas" (e.g. Γ) are amplitudes related to the specific heat.

Using the relations introduced above we want to compute the correlation length for carbon dioxide along the coexistence diameter $\widehat{\rho}_d = 0$ ($t > 0$), along the critical isotherm $t = 0$, and along coexistence states $\widehat{\rho}_{g/l}$. Ref. [26] provides the experimental values for $B = 1.59(3)$ and $f_+ = 1.50(9)$Å. The last allows –using Eq. (A2)– to compute the correlation length along the supercritical coexistence diameter within a 6% errorbar. Using the universal amplitudes and the experimental values of f_+ and B, we can easily compute also the correlation length at coexistence ξ_c and along the critical isotherm $\xi_{t=0}$

$$\xi_c(\widehat{\rho}) = \frac{f_+}{\mathbf{U}_\xi} B^{\frac{\nu}{\beta}} (\widehat{\rho})^{-\frac{\nu}{\beta}} \qquad \xi_{t=0} = f_+ \left(\frac{\mathbf{Q}_2}{\delta \mathbf{R}_\chi}\right)^{\frac{1}{2-\eta}} B^{\frac{\nu}{\beta}} (\widehat{\rho})^{-\frac{\nu}{\beta}} \quad . \tag{A13}$$

Notice that at fixed ρ the ratio between the correlation length along the critical isotherm and along the coexistence states is universal and given by $\mathbf{U}_\xi \left(\frac{\mathbf{Q}_2}{\delta \mathbf{R}_\chi} \right)^{\frac{1}{2-\eta}} \approx 0.73$.

Using Eq. (A13) and (A2) in Fig. 10 we sketch lines at constant correlation length. Starting from previous obtained results along the coexistence diameter, the critical isotherm and the coexistence densities we interpolate these points using simple quadratic functions (hyperbola). This is an approximation, indeed the correct way to proceed would require the knowledge of an universal crossover function $f_\xi(x)$ which interpolates the correlation length in the full $(\widehat{\rho}, t)$ plane [27].

[1] Kiran, E., and Brennecke, J. F., eds., 1993, *Supercritical Fluid Engineering Science. ACS Symposium Series 514* (Washington D.C: American Chem. Soc.). Kiran, E., and Levelt-Sengers, J. M. H., eds., 1994, *Supercritical Fluids* (Dordrecht: Kluwer).

[2] Kemmere, M. F., and Meyer, Th., eds., 2005, *Supercritical Carbon Dioxide in Polymer Reaction Engineering* (Weinheim: Wiley-VCH).

[3] Levesque, D., Weis, J. J., and Hansen, J. P., 1979, in *Monte Carlo Methods in Statistical Physics,* edited by K. Binder, **7**, 47.

[4] Frenkel, D., Smit, B., 2002, *Understanding Molecular Simulation: From Algorithms to Applications* (San Diego: Academic Press)

[5] Landau, D. P., and Binder, K., 2005, *A Guide to Monte Carlo Simulations in Statistical Physics* (Cambridge: University Press).

[6] Scott, R. L., and van Konynenburg, P. H., 1970, Discuss. Faraday Soc., **49**, 87; van Konynenburg, P. H., and Scott, R. L., 1980, Philos. Trans. R. Soc. London Ser. A, **298**, 495; Rowlinson, J. S., and Swinton, F. L., 1982, *Liquids and Liquid Mixtures*, (London: Butterworths).

[7] Bolz, A., Deiters, U. K., Peters, C. J., and de Loos, T. W., 1998, Pur. Appl. Chem., **70**, 2233.

[8] Levesque, D. and Weis, J. J., 1991, in *The Monte Carlo Method in Condensed Matter Physics,* edited by K. Binder, **71**, 121.

[9] Krause, B., Sijbesme, H. J. P., Münüklü, P., van der Vegt, N. F. A., and Wessling, M., 2001 Macromolecules, **34**, 8792.

[10] Yip, S., ed., 2005, *Handbook of Material Modeling* (Berlin: Springer).

[11] Kotelyanskii, M. J., Theodorou, D. Y., eds., 2004, *Simulation Method for Polymers* (New

York: Marcel Dekker).

[12] Mognetti, B. M., Yelash, L., Virnau, P., Paul, W., Binder, K., Müller, M., and MacDowell, L. G., 2008, J. chem. Phys., **128**, 104501.

[13] Mognetti, B. M., Oettel, M., Yelash, L., Virnau, P., Paul, W., and Binder, K., 2008, Phys. Rev. E, **77**, 041506.

[14] Gelb, L. D., Müller, E. A., 2002, Fluid Phase Equilib., **203**, 1; Albo, S., Müller, E. A., 2003, J. Phys. Chem. B, **107**, 1672; Müller, E. A., Gelb, L. D., 2003, Ind. Eng. Chem. Res., **42**, 4123.

[15] Virnau, P., Müller, M., MacDowell, L. G., and Binder, K., 2004, J. chem. Phys., **121**, 2169.

[16] Mognetti, B. M., Yelash, L., Virnau, P., Paul, W., Binder, K., Müller, M., and MacDowell, L. G., 2008, J. chem. Phys., *to appear*; Binder, K., Mognetti, B. M., Macdowell, L. G., Oettel, M., Paul, W., Virnau, P., and Yelash, L., Macromol. Symposia, *submitted*.

[17] Levesque, D., Weis, J. J., and Hansen, J. P., 1984, in *Application of the Monte Carlo Method in Statistical Physics,* edited by K. Binder, **36**, 37.

[18] Mognetti, B. M., Virnau, P., Yelash, L., Paul, W., Binder, K., Müller, M., and MacDowell, L. G., 2009, Phys. Chem. Chem. Phys., DOI:10.1039/b818020m

[19] Stell, G., Rasiaiah, J. C., and Narang, H., 1974, Mol. Phys., **27**, 1392.

[20] NIST website: http://webbook.nist.gov/chemistry/

[21] Sato, T., Sugiyama, M., Misawa, M., Takata, S., Otomo, T., Itoh, K., Mori, K., and Fukunaga, T., 2008, J. Phys.: Condens. Matter, **20**, 104203.

[22] Nishikawa, K., Tanaka, I., Amemiya, Y., 1996, J. Phys. Chem., **100**, 418.

[23] Ishii, R., Okazaki, S., Okada, I., Furusaka, M., Watanabe, N., Misawa, M., and Fukunaga, T., 1996, J. chem. Phys., **105**, 7011.

[24] Adams, J. E., and Siavosh-Haghighi, A., 2002, J. Phys. Chem. B, **106**, 7973.

[25] Hansen, J. P., and McDonald, I. R., 1986, *Theory of Simple Liquids* (New York: Academic).

[26] Sengers, J. V., Moldover, M. R., 1978, Phys. Lett. A, **66**, 44.

[27] Pelissetto, A., Vicari, E., 2002, Phys. Rep., **368**, 549.

[28] Harris, J. G., and Yung, K. H., 1995, J. Phys. Chem., **99**, 12021.

[29] Murthy, C. S., Singer, K., and McDonald, I. R., 1981, Mol. Phys., **44**, 135.

[30] Chiappini, s., Nardone, M., Ricci, F. P., and Bellissent-Funel, M. C., 1996, Mol. Phys., **89**, 975; Cipriani, P., Nardone, M., and Ricci, F. P., 1998, Physica B **241-243**, 940; Cipriani, P.,

Nardone, M., Ricci, F. P., and Ricci, M. A., 2001, Mol. Phys., **99**, 301.

[31] Murad, S., Gubbins, K. E., and Gray, C. G., 1979, Chem. Phys. Lett., **65**, 187; Lee, L. L., Assad, E., Kwong, H. A., Chung, T. H., and Haile, J. M., 1982, Physica, **110A**, 235; Murad, S., Gubbins, K. E., and Gray, C. G., 1983, Chem. Phys., **81**, 87.

[32] Temleitner, L., and Pusztai, L., 2007, J. Phys.: Cond. Mat., **19**, 335203.

[33] Shukla, C. L., Hallett, J. P., Popov, A. V., Hernandez, R., Liotta, C. L., and Eckert, C. A., 2006, J. Phys. Chem. B, **110**, 24101

[34] Fisher, M. E., 1974, Rev. Mod. Phys., **46**, 597.

[35] Privman, V., Hohenberg, P. C., Aharony,A. in *Phase Transitions and Critical Phenomena, vol. 14*, Domb, C., Lebowitz, J. L., eds., 1991 (Academic Press).

[36] Caselle, M., Hasenbusch, M., 1997, J. Phys. A, **30**, 4963.

[37] Fisher, M. E., Zinn, S.-Y., 1998, J. Phys. A, **31**, L629.

[38] Zalczer, G., Bourgou, A., Beysens, D., 1983, Phys. Rev. A, **28**, 440.